Hawassa University Journals

Volume II
Pages: 1-24
Article Number: 775-Research Results-3726-1-2-20230202

www.journals.hu.edu.et/hu-journals/index.php/ejet/index

Ethiopian Journal of Engineering and Technology

A Study of Aerodynamic Pressure Drag and Skin Friction Resistance Comparison on ICE 3 Train under Different Yaw-angles

Kibret Yilak Molla

Email: kibretyilak2005@gmail.com; **ORCID**: https://orcid.org/0000-0002-0695-1793

Department of Mechanical Engineering, Institute of Technology, University of Gondar, Gondar, Ethiopia.

Abstract: A chief purpose of this research has presented for comparison of the aerodynamic pressure drag and train body skin friction resistance contribution on ICE 3 HST vehicles, which run at 320km/h speed. It has also determined the flow character at each car on the train according to their position. The two main factors of external HST body resistance have been studied in different yaw-angle conditions of open embankment infrastructure. The full-scale test is conducted to verify the computer, mesh, and a serious numerical simulation to the performed investigation of aerodynamic loads for comparison pressure drag and frictional resistances. Has used PHOENICS VR CFD numerical test approach, and validated by EN14067-6:2010 standard report and experimental test values in Table 9. For applying in the LES turbulence model, a blockage ratio of 3.015% and at Reynold's maximum number of 1.120E+08. From the detailed flow analysis, the research found out that pressure drag is the dominant air resistance compared to train body skin friction. Especially, it showed that the frictional resistance became much less when the wind attack angles different from zero. Particularly, which are from drag components, the maximum pressure drag in the x-axis recorded when a wind yaw-zero and which is decreased as the wind yaw-angle attack increased. That has illustrated in Table 8 from the range of 22.45% for a minimum of 10.53%. But, the side force is increased by 66.36% to a maximum of 97.38%. And also, the lift force was recorded higher at yaw-zero and dropped in a very noticeable effect from case-1 to case-2 tests by 98.48%. On the other hand, it started to increase gradually while the wind yaw-angle increased, which was in the range of 21.64% to a maximum of 69.15%. Hence, the study predicted that the running stability of the ICE3 train going to worse when the wind attack yaw-angle increased. This owes to lift and side force coefficients drastically rose. The study clearly has provided that the aerodynamics pressure drag is dominant over friction resistance when an HST running under an incompressible medium.

Keywords: Aerodynamic resistance, Pressure load, Friction load, High-Speed Train, and Train.

1. Introduction

In railway transportation operations, at rolling stock, there are two kinds of train operational resistance that are mechanical and aerodynamics. For HST aerodynamics load resistance is inevitable and more

dominant. This study focused on the aerodynamic resistance to energy efficiency and further investigation of its impact on HST cars at open air. It's significantly depend on the train operating velocity and yaw-angle effects, and that conducted in the open air with no structure presented at embankment rail-track. This can be explained the contribution of aerodynamic load resistance by two main factors and compared their values. Those are; *aerodynamic pressure drag resistance* which is depend on the train vehicle speed, body shape, train length and cross-sectional area, track type and line system environment, headwind, air density and others. And *aerodynamic train vehicle's body surface friction*; which is very important to consider in HST application when train speed is higher and higher that's closed to compressible fluid flow situations. As this study result found out that pressure drag is the dominant resistance force. Besides, the high-speed train running instability has influenced by factors of different yaw-angles and flow around a train bodies has also explained. The study conducted in a full-scale and a 3D incompressible turbulent flow at steady state numerical simulation test.

A lot of train overturning accidents occurring from time to time. Typically, train car derailment under gust or windy environment operation lines have been reporting around the world frequently. As the result showed that the train could be vulnerable to undesired lift and side force. That's when train running on the open track, cross-wind and headwind load resistance are unavoidable, and the train becoming more instable as the wind yaw-angle increase. That's the most prominent approach to assess a resistance of train by full-scale test has advantages for determine the flow profile at each car accordingly. Particularly, for high-speed-train types. It's supported by European legislation within the framework of the TSI, RSSB and other EN-standards(Coming, 2006; Commission, 2019; En, 2005; European Commission, 2003; RSSB, 2009)Most researches have been conducting to predict and assess an aerodynamic load effect on HST by reducing a small scaled and single model, or two models, and some scholars used three model cars in the test. That's because of saving the test economies and computational times. But, the results could be overestimate or mislead in some way with compare to experimental values. Those tests are wind tunnel experimental or computational dynamics numerical simulation test and both.

This study has been proposed from a recent study on simulation for flow around HST review for future work. The authors suggested that for reasonable simulation result; details of trains' geometry including all cars, wall-based approach methods, and to reduce meshing errors will be use more accurate values by Mohammed M. et al. (Mohammad Mehdi Rashidi; Alireza Hajipour; Tian Li; Z. Yang; Qiliang Li, 2019) in 2019. Hence, this paper approached at full-scaled model train set that can give detail investigation of aerodynamic force impacts and flow characteristics on each car. It compared and found out the dominant resistance factor in the given situations. Besides, the determination of stability against overturning at standstill train set models can be explained, which

could be unavoidable of increasing of lift force and side force when the wind yaw-angle becomes large. It's also supported by other train aerodynamic review studies(C. Baker et al., 2009; C. J. Baker, 2014a, 2014b; Kumar et al., 2016; Mueller & DeLaurier, 2003; Raghunathan et al., 2002; Tian, 2019)The analysis of wind load must have considered static and buffeting loadings. For the directions of wind loads, it includes the pressure drag and skin friction drag forces, lift force and pitch moment are also more important to train stability analysis. Besides, train car either overturning or derailment is the main factor of incident, owing to cross-wind. Particularly, the wheel unloading depend on the train speed, wind angle and uncompensated lateral acceleration effects can be mainly considered. These days, for the purpose of cross-wind reduction at open track line section of HST operation, the newly arranged railway systems are installing wind barriers that could be more safety proofed. But that's not economical for long line system. Sun et al. (Sun et al., 2019) in 2019, investigated when high-speed train passing on the breach, a sudden increasing aerodynamic load and the first wheelset compel to yaw toward the windward side occurred. Diedrichs (Diedrichs, 2003) in 2003, described the flow on ICE2 train of leading two cars using CFD and Diedrichs et al. (Diedrichs et al., 2007) in 2007, also presented the influence of cross-wind on ICE2 train at embankment. Schobe et al. (Schober et al., 2010) in 2010, investigated that in the wind tunnel test of ICE3 aerodynamic force and moment has strongly depend on the ground configurations. It recommended for the determination of aerodynamic forces acting on a train on three different ground configurations, to measure the aerodynamic coefficients. In addition, the influence of cross-wind on HST and its implication has covered in (Avila-Sanchez et al., 2014)(Bagherwal, 2018; Cheli et al., n.d., 2010; Huo-yue et al., n.d.; Noguchi et al., 2019; Sanquer et al., 2004; Yu et al., 2019) studies.

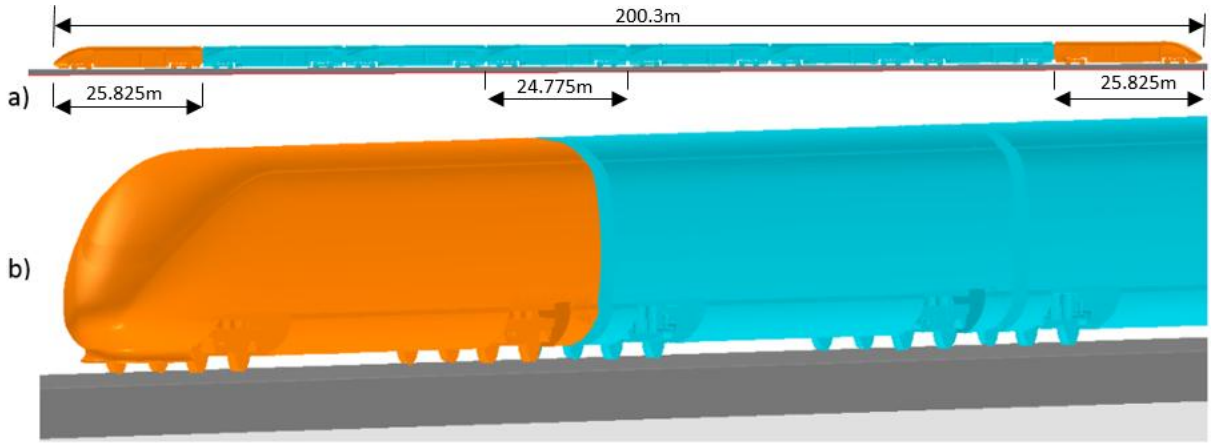

Figure 1: ICE3 Train Model at 100mm embankment.

However, the previous of either ICE2 or ICE3 train studies only considered two car models. In this study as shown the model in Figure 1, to determine the aerodynamic pressure and friction force's

coefficients, and explained the flow characteristic of wind at each car, applied PHOENICS VR numerical simulation program.

Hence, based on the aforementioned descriptions, this study tried to compare the two main aerodynamics resistance loads of an ICE3 high-speed train' ae at embankment open track. It focused on the following subjects to be considered.

- Comparison of pressure drags and skin friction resistance values at different yaw-angles.
- The significant impact of aerodynamic resistance profile at each train car and their parts.
- The embankment effects on the train system at different yaw-angle.

This study has regarding the effects of steady aerodynamic loads resistances at one-meter embankment and exposed to different yaw-angle wind flowing. The analysis presented into two categories. It is mainly concerned that comparison of the aerodynamic force pressure drag and friction resistance, and characteristics of the flow field by using computational fluid dynamics program, which neglected the wheel–rail interaction.

This research, according to EN 14067-6:2010 standard, the requirement and test procedure for assessments are considered, and blockage ratio for numerical simulation of CFD study is less than 10% (that is 3.015%). So that no needed blockage correction test. The test conducted in an open embankment environment system as shown in Figure 3. The analysis was conducted within different yaw-angles and analyzed the aerodynamic flow around a train bodies. It also applied in LES turbulence model, and at Reynold's maximum number of 1.120E+08.

2. Analysis of aerodynamic loads and moments

According to general aerodynamic force and moment principles aerodynamic coefficients, which are non-dimensional numbers, have used to determine the aerodynamic characteristics. When a train is subjected to external air resistance, aerodynamic forces and moments can be defined in Eq. 1&2 respectively.

$$F_i = \frac{1}{2} \cdot \rho \cdot C_{Fi} \cdot A \cdot |V + U|^2 \qquad \text{For i = x, y\&z} \qquad (1)$$

$$M_i = \frac{1}{2} \cdot \rho \cdot C_{mi} \cdot A \cdot L \cdot |V + U|^2 \qquad \text{For i = x, y\&z} \qquad (2)$$

2.1 Aerodynamic resistance loads on high-speed train

The main aerodynamic load factors are pressure drag and skin friction with stress distribution on the running train body. Typically, for high-speed trains can form of a drag, lateral and life force, and a moment of yawing, pitching and overturning are always occurring on the running railway vehicles. The magnitude is depending on the type of train vehicle external body shape, the speed of train and as well the environmental wind situations on an open track line. In this study, as shown in Figure 2 of ICE3 High-speed train leading car top view model at open and embankment track, trying to explain its wind to train relative velocity representations. That's to understand the velocity diagram at some different yaw-angle situations.

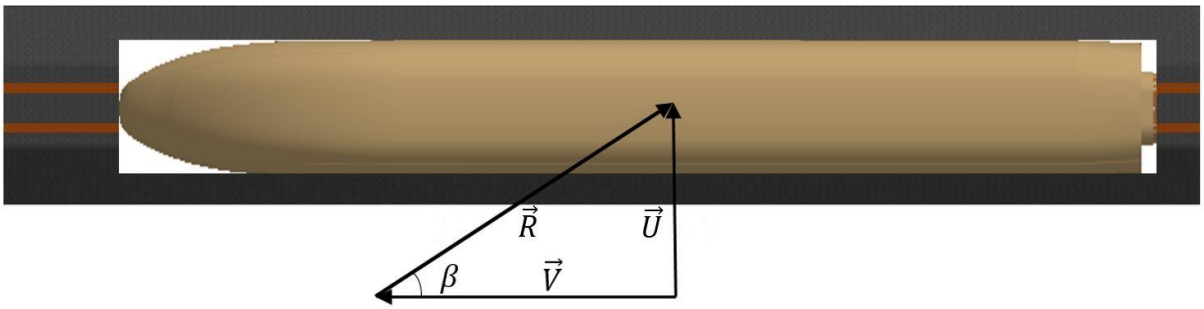

Figure 2: Velocity diagram of ICE 3 High-Speed Train leading Car at CFD Simulation.

As shown in the Figure 2 velocity diagram; the train speed (V), wind speed (U) and the wind direction relative to train at angle of β are explained. This study assumed that conducted at steady and constant maximum vehicle speed model, which is 320km/h. In this case, the variable yaw-angle (β) can be defined in Eq. (3).

$$\beta = \tan^{-1}(\frac{U}{V}) \qquad (3)$$

3. The track embankment layout and its effect on the CFD simulation

The aerodynamic studies of HST have been done by many researchers. Which has been included the cross-wind influence on it either in wind tunnel or numerical simulation tests as a single and scaled model. Those, the scaled and one or two car model tests, couldn't give enough assessment of a velocity and pressure profile effects on embankment, and on the whole system of train cars. Some typical train operation line sections of the open embankments, viaducts, curved tracks and bridges are likely vulnerable to aerodynamic loads. These probably increase the risk of train overturning under environmental wind scenarios more than true flat ground platform. So, this paper has considered and analyzed the track embankment effects into the train aerodynamic resistance and stability. According to EN 14067-4 (*E P U B L I C O F U L G a R I A*, 2009) aerodynamics on open track test procedures that can be give us the insight pressure and velocity profiles on ICE 3 full scaled high-speed train

system Figure 1 to show aerodynamic load effects in detail. It's also described as Figure 3 embankment track cross-sectional and front view of train.

4.

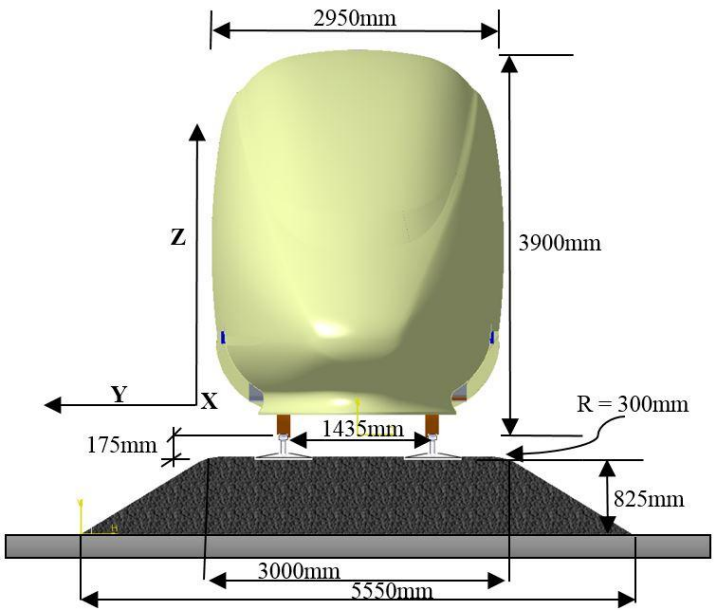

5.

Figure 3: The standard aerodynamics test on a single-track sectional views and ICE 3 high-speed train front side.

4. Numerical Test procedures

4.1 PHEONICS

It's a general-purpose software package which uses the techniques of CFD, which can predict the simulation test both quantitatively and qualitatively that how fluids flow in and around the objects. This program has some unique feature like, fine-grid embedding in the Virtual-Reality interface, that helps to local grid refinement is possible when a structured grid is in use. In this study, the flow, around the train cars, is usually subjected to the following characteristics; three-dimensionality, high Reynolds number, turbulence, deceleration and acceleration, curved boundaries, separation, possible reattachment, recirculation, and swirling properties. Therefore, this study used PHOENICS to compare the aerodynamic resistances on ICE3 train set. The model which the proper solution of this aerodynamic problem determined by LES (Large Eddy Simulation).

4.2 ICE 3 High-Speed Train Model parameters

Table 1: ICE 3 High-Speed Train Specifications.

Parts	Descriptions	Values

Train-set	• Overall dimensions of each Car's and gross weight of train • Cars' length including of half of coupling length	Length of lead and end car(25.825m) Length of mid_cars(24.775m) Height (3.90m) Width (2.95m)
Speed	Maximum operating speed	320km/h
Power Supply	Electric System	15kv AC
Power output	Tractive effort	8,000KW
Length	Total length of train	200.3m
Gap b/n Cars	Coupling length	0.6m
Weight of train	The train set	409t

4.3 Initial boundary conditions and Computational domain

The initial input data for the CFD test, and the ICE3 model were given by the full scale.

Table 2: Initial boundary conditions for CFD simulation test.

Boundary	**Boundary conditions**	**Values**
Inlet	Constant velocity	320km/h
Area	Reference area	$10m^2$
Length	Reference normalization length	3m
Outlet	Pressure outlet	Pressure is P = 0 N/m^2
Ground	Embankment Track	Stationary
Train Model	Train set	Stationary
Wind inlet	Velocity at β yaw-angle from track side plane	Constant velocity
Right-side wall outlet	Pressure outlet	Ambient pressure is P = 0 N/m^2
Control volume Domain Size	3D dimension of Virtual wind tunnel X,Y and Z	X = 2000m, Y = 65.55m Z = 30m
Air	Reference moving air density at 20°c	ρ = 1.2041kg/m^3
CG	Location at the middle area of car	Height = H/2 Length= L/2

For this study, the computational domain, boundary conditions, the blockage ratio, turbulence modelling and meshing of the model shouldn't have interfered with the flow around the train in a physical incorrect way. The model of the train set and control volume configuration for test has prepared and presented in Figure 4.

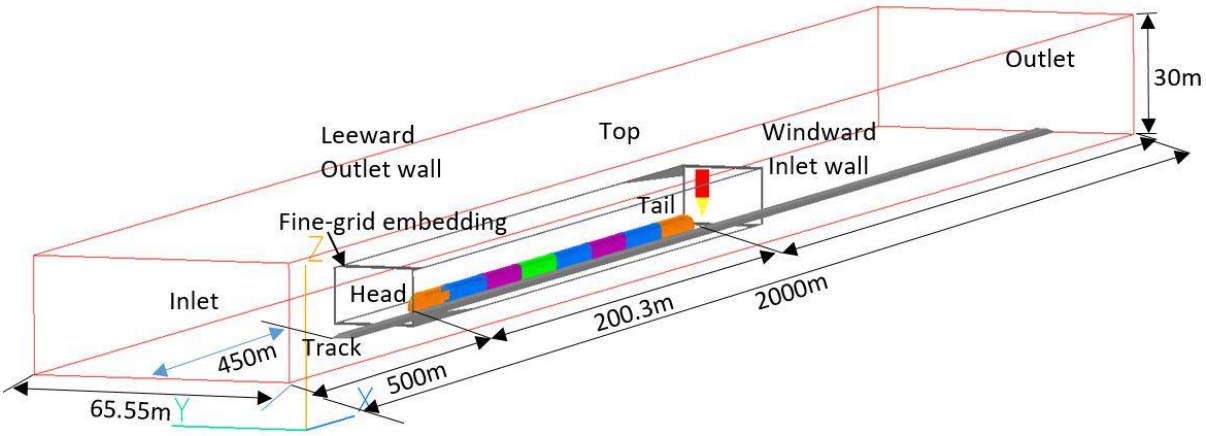

Figure 4: The virtual computational domain of the considered train model configuration.

4.4 Computational and mesh sensitivity

Mesh independency tests have conducted accurately to control the geometric complex in the domain as shown in Figure 5. It's a numerical sensitivity of that can control the fluctuation of the pressure, velocity and all other values regarding meshes grid density. Some preliminary tests should be necessary till the flow velocity and pressure profile values almost constant at a certain maximum meshing level. For this study, meshes have shown good agreement in both flow topology, and force and moment coefficients. In this case, the fine grid volume can help the local resolution of flow around the train. The three principal views are illustrated below in the Figure 5.

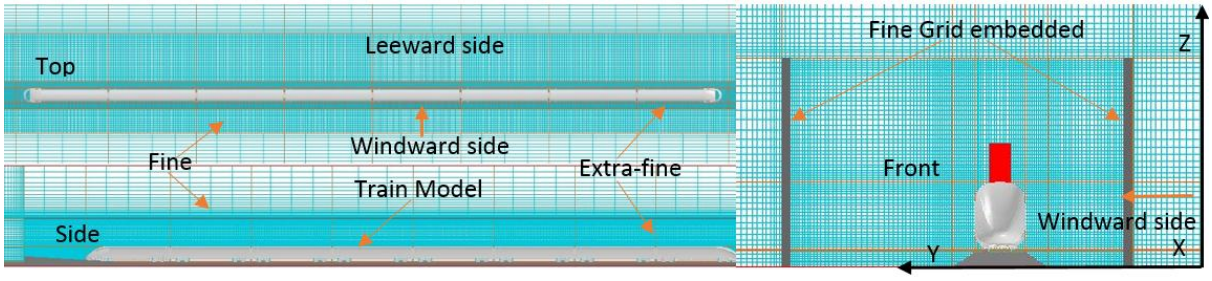

Figure 5: Overall grid structure for test from front and side views

5. Result and discussions

5.1 Pressure drag and train car bodies' surface friction resistance

The flow profiles analyses of this study has illustrated from Figure 6 to Figure 15 and Table 3 to Table 7 that the flow regions where high pressure and friction resistances in cars are explained below. Which have separated analysis for train set and each car at different yaw-angle situations. Besides,

those boundary layers, large vortex structures, recirculation zones, stagnation zones, separation and wake areas can be also seen clearly. Particularly, the study interest has compared the pressure and friction contribution on ICE3 HST in both qualitatively and quantitatively at varied yaw-angle.

The pressure loads are the dominant and significant than skin friction resistance in all five cases of the study. Which also showed that the leading and end cars got a strong plosive and negative drag resistance respectively when the yaw wind angle was zero-degree. Moreover, the friction force generated on train car's body surface with interaction wind loads at yaw-angle zero is more noticeable than compared to other cases.

5.1.1 Case_1: Flow distributions at zero yaw-angle (β =0°)

In this case, the pressure drag load through x-axis is the more dominant over other pressure drag. Similarly, x-axis friction resistance load is dominant over others. And the most importantly, the flow structure around train cars has clearly investigated and categorized into; high pressure with air stagnant region on the front of leading car indicated in Figure 6, Figure 7 and Table 3 which extended to the end of the first bogie parts of the body, wake regions occurred at the end car and underbody surface on both first and last car, the steady flow region happed in car-2, 3 and 4, the low pressure region occurred after car-5. Besides, on the track which are in front of leading car and behind of the end car showed strong positive and negative load effects. However, the track-air r interaction has excluded from train-air interaction in study, as Figure 6d&f explained that there is train-embankment interaction of pressure bouncing from train car bodies to embankment and the vice versa. Which could be more exacerbated the lift and side forces that has negative impacts on train running stability. Moreover, as the results explained this train-embankment interaction through air pressure load could be causes of vortex generation. Typically, at underbody structures, leeward side, coupling systems and top of train car's body which can be cause of more pressure resistance. Therefore, improving train-embankment interactions and wake regions can help to reduce the pressure drag significantly.

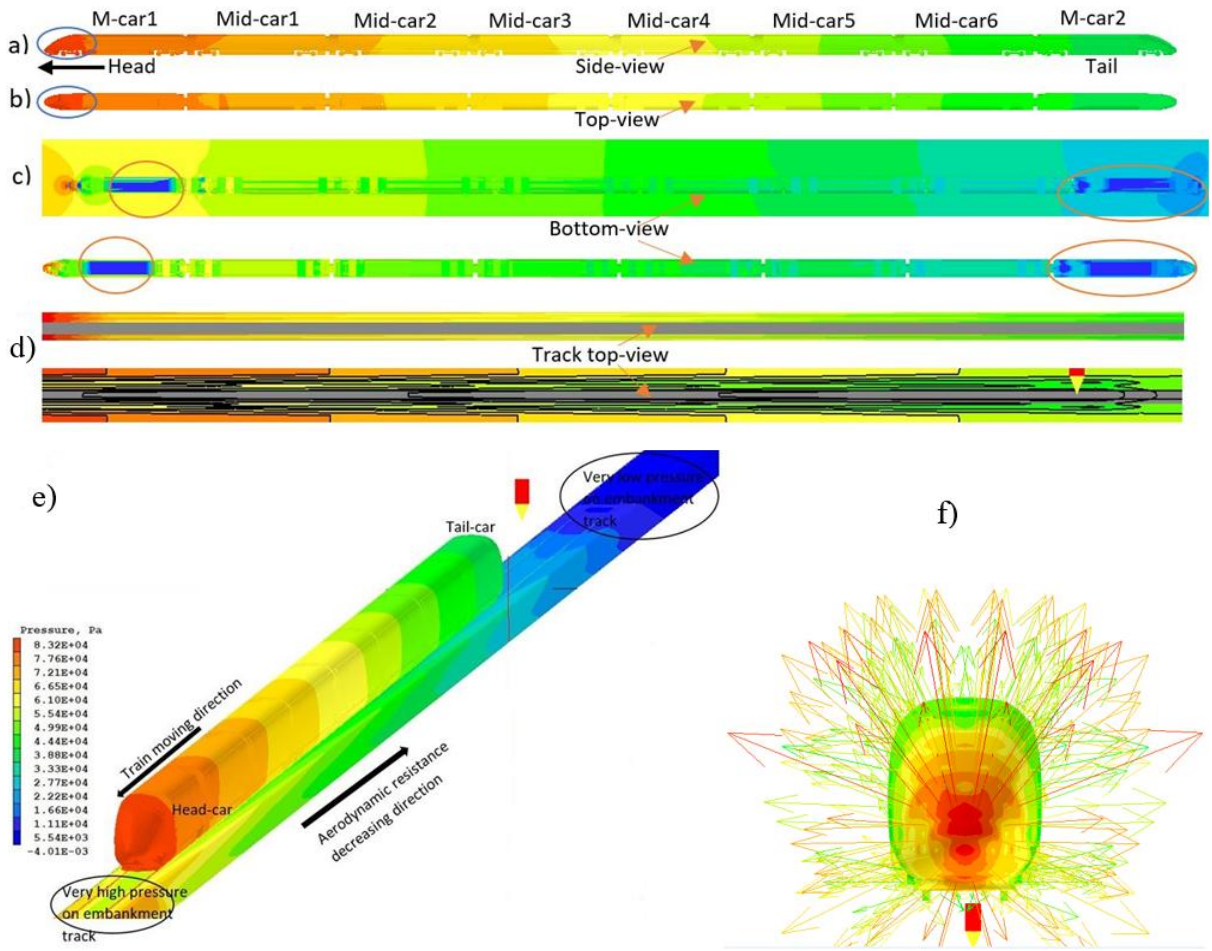

Figure 6: Aerodynamic resistance load distribution on ICE3 full-scaled train at β = 0°

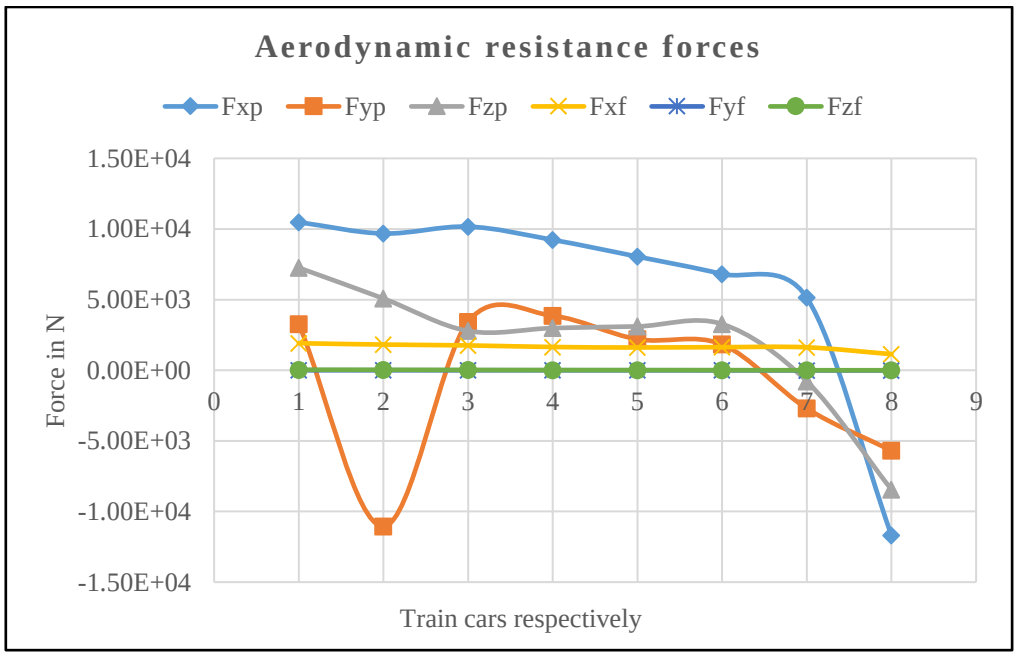

Figure 7: Comparison of the aerodynamic resistance forces value for each car at β = 0°

Table 3: Comparison of the aerodynamic resistance force values for each car at β = 0°

Car type In the Train set	**Pressure Force (F_P) in N**			**Friction Force (F_f) in N**		
	Fxp	Fyp	Fzp	Fxf	Fyf	Fzf
Leading car_1	1.048033E+04	3.275590E+03	7.258554E+03	1.912355E+03	1.857709E-01	3.698024E+01
Mid_Car_2	9.680984E+03	-1.10539E+04	5.078539E+03	1.818026E+03	2.212448E+00	3.181965E+01
Mid_Car_3	1.016800E+04	3.432447E+03	2.780611E+03	1.758405E+03	-4.27935E-01	2.172190E+01
Mid_Car_4	9.231422E+03	3.850204E+03	2.989911E+03	1.645634E+03	-6.35474E-01	1.451492E+01
Mid_Car_5	8.045719E+03	2.194124E+03	3.102225E+03	1.610771E+03	-2.51524E+00	1.072680E+01
Mid_Car_6	6.810180E+03	1.830365E+03	3.269979E+03	1.634665E+03	-3.31425E+00	7.198688E+00
Mid_Car_7	5.140836E+03	-2.70167E+03	-7.82858E+02	1.623620E+03	-9.31717E+00	7.659696E-01
End car_8	-1.168487+04	-5.68695E+03	-8.44891E+03	1.140173E+03	-1.26729E+01	3.745345E-01

5.1.2 Case_2: Flow distributions at yaw-angle(β = 15°)

As Table 4 and Figure 8&9 has presented that the pressure side force those are in the y-axis are the dominants, and the impact goes through, almost the same till the car-5 and then decrease for on the last two cars accordingly. However, the pressure drag effects through x-axis lower than side force values, in this case relatively the maximum values occurred from car-3 to car-7. Only the maximum positive lift force occurred at car-8, and also negative significant lift force happed at Car-2 and Car-7. Comparatively, friction loads are very much less in all directions. Therefore, it provided that to show the pressure forces are strongly much dominant than friction loads on the train cars' body.

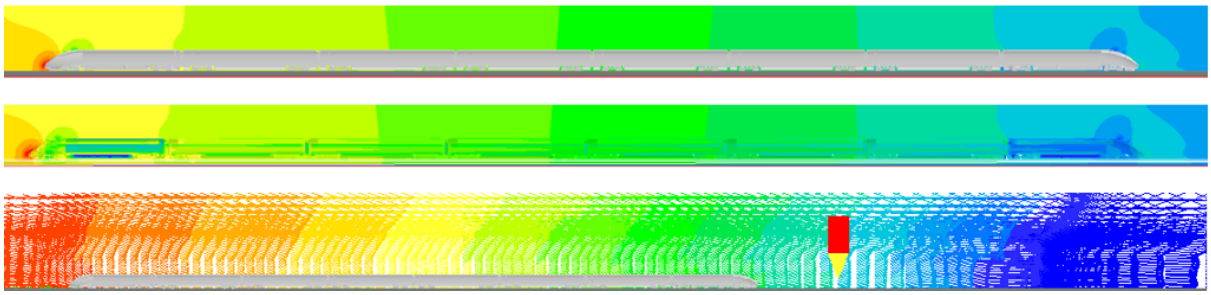

Figure 8: Aerodynamic resistance load distribution on ICE3 full-scaled train at yaw-angle β = 15°

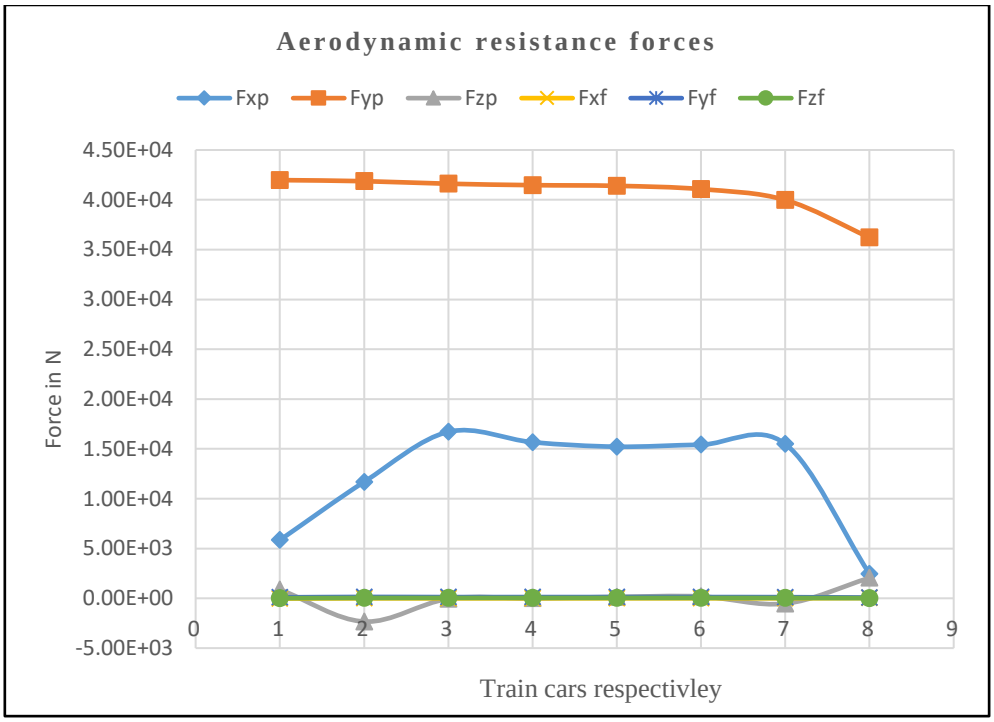

Figure 9: Comparison of the aerodynamic resistance forces value for each car at β = 15°

Table 4: Comparison of the aerodynamic resistance force values for each car at β = 15°

Car type	**Pressure Force (F_P) in N**			**Friction Force (F_f) in N**		
	Fxp	Fyp	Fzp	Fxf	Fyf	Fzf
Leading car_1	5.841682E+03	4.197476E+04	8.801295E+02	1.330591E+01	9.608435E+01	-5.30609E-01
Mid_Car_2	1.168329E+04	4.186868E+04	-2.335241E+03	3.387724E+01	1.349649E+02	-2.28768E+01
Mid_Car_3	1.670528E+04	4.161120E+04	-5.119329E+01	3.574776E+01	1.194195E+02	-1.95142E+00
Mid_Car_4	1.566611E+04	4.147059E+04	2.589932E+00	3.605138E+01	1.230445E+02	1.234837E+00
Mid_Car_5	1.521730E+04	4.139952E+04	1.417389E+02	3.550719E+01	1.228072E+02	3.484412E+00
Mid_Car_6	1.541849E+04	4.106904E+04	1.849703E+02	3.572083E+01	1.217483E+02	4.281838E+00
Mid_Car_7	1.548844E+04	3.998056E+04	-5.340822E+02	3.346379E+01	1.139227E+02	8.645213E+00
End car_8	2.460406E+03	3.621798E+04	2.045940E+03	1.589817E+01	7.250008E+01	2.825697E+01

5.1.3 Case_3: Flow distributions at yaw-angle (β = 30°)

As the pressure contour illustrated in Figure 10, Figure 11 and Table 5 that the loads became harder due to increasing of wind yaw-angle. The train cars particularly from car-3 to car-6 got more hit toward the side than train run direction. Compared to case-2 test, the magnitude of pressure loads in case-3 more larger values recorded. Even though, the friction loads toward y-axis increased than

previous case-2, it's still negligible compared to pressure drags. Thus, as the same pattern of case-2 the pressure drags force values increased.

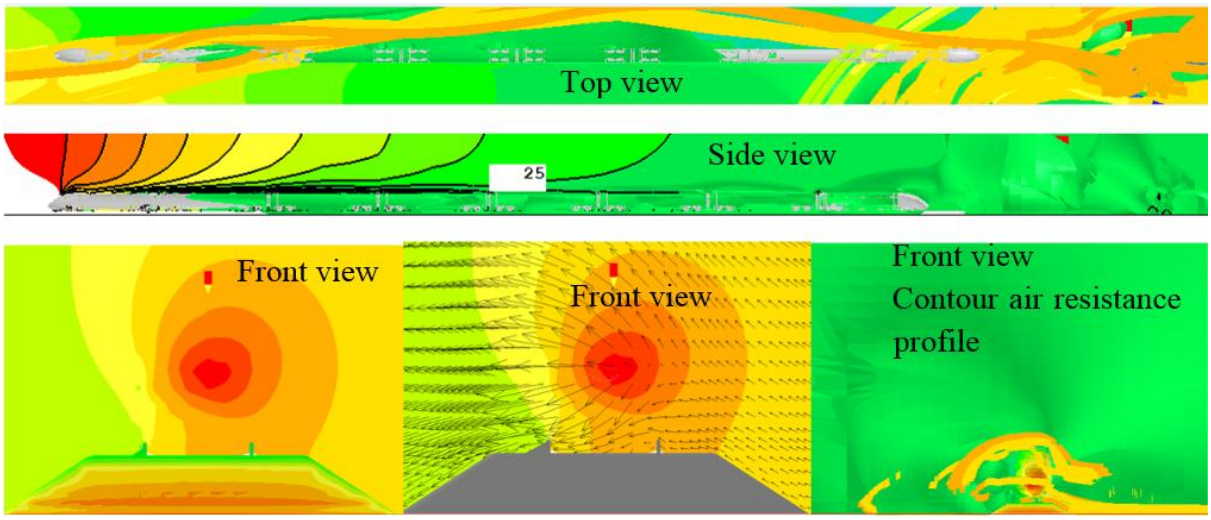

Figure 10: Aerodynamic resistance load distribution on ICE3 full-scaled train at yaw-angle β = 30°

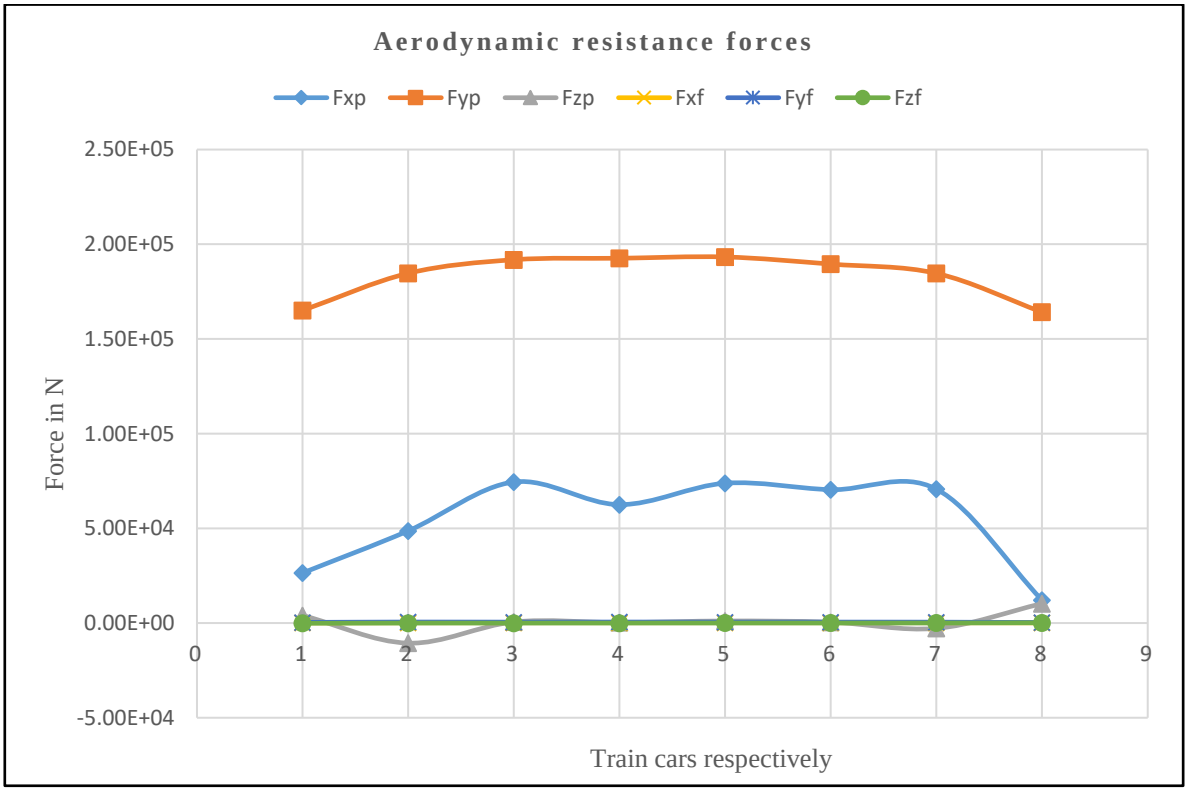

Figure 11: Comparison of the aerodynamic resistance forces value for each car at β = 30°

Table 5: Comparison of the aerodynamic resistance force values for each car at β = 30°

Car type	**Pressure Force (F_P) in N**			**Friction Force (F_f) in N**		
	Fxp	Fyp	Fzp	Fxf	Fyf	Fzf
Leading car_1	2.645037E+04	1.650849E+05	4.028761E+03	5.890474E+01	3.481459E+02	-2.02797E+01
Mid_Car_2	4.867783E+04	1.846851E+05	-1.061107E+04	1.316964E+02	5.295439E+02	-1.25418E+02
Mid_Car_3	7.447194E+04	1.918426E+05	5.735073E+02	1.462785E+02	4.907702E+02	-8.97994E+00
Mid_Car_4	6.253188E+04	1.926193E+05	2.450461E+02	1.444649E+02	5.287277E+02	4.080713E+00
Mid_Car_5	7.383434E+04	1.932909E+05	1.081483E+03	1.491051E+02	5.030475E+02	1.537728E+01
Mid_Car_6	7.041883E+04	1.895239E+05	4.532711E+02	1.447183E+02	5.030206E+02	1.757680E+01
Mid_Car_7	7.067202E+04	1.846322E+05	-2.811547E+03	1.397242E+02	4.760675E+02	3.794287E+01
End car_8	1.206072E+04	1.641648E+05	1.028171E+04	6.477841E+01	3.003291E+02	1.268235E+02

5.1.4 Case_4: Flow distributions at yaw-angle (β = 45°)

Although the overall pressure resistance loads became larger than case-3 in all directions, the pressure loads in y-axis as well as x-axis started increasing from car-1 to car-3 and decreased from car-5. But, the lift forces have the same fashion from case-2 and case-3 except which recorded more magnitudes. So, we can be agreed that there is more pressure load exist when the wind yaw-angle different from zero. This could be increasing instability of train cars. As Figure 12 and Table 6 illustrated that each car got strong pressure hit towards y-axis. Besides, the friction resistance loads larger than all the previous cases.

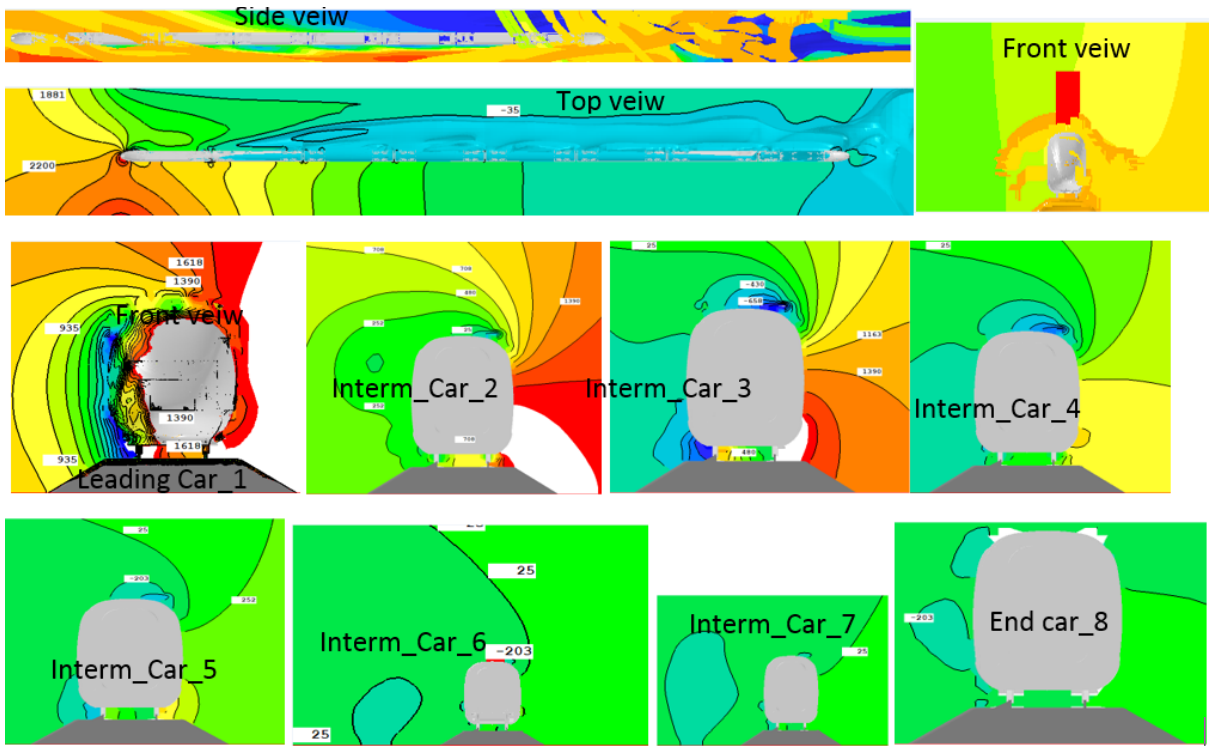

Figure 12: Cross-sectional car body's aerodynamic resistance load distribution on ICE3 full-scaled train at yaw-angle β = 45°

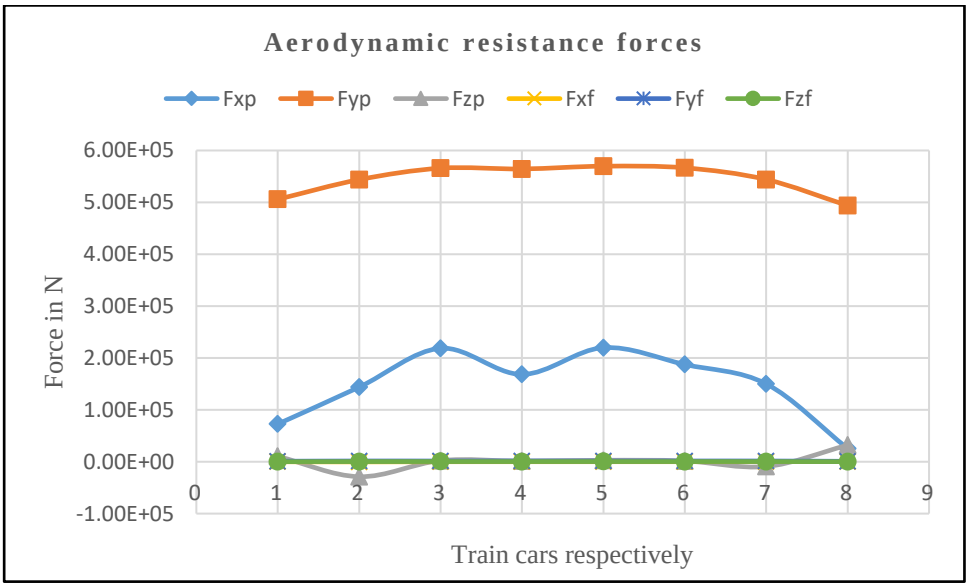

Figure 13: Comparison of the aerodynamic resistance forces value for each car at β = 45°

Table 6: Comparison of the aerodynamic resistance force values for each car at β = 45°

Car type	Pressure Force (F_P) in N			Friction Force (F_f) in N		
	Fxp	Fyp	Fzp	Fxf	Fyf	Fzf
Leading car_1	7.266559E+04	5.058642E+05	1.034311E+04	-6.256406E+01	9.545233E+02	1.5145E+02
Mid_Car_2	1.438333E+05	5.438058E+05	-2.879785E+04	-3.425312E+02	1.450388E+03	3.6455E+02
Mid_Car_3	2.186252E+05	5.658601E+05	2.230593E+03	-1.472743E+01	1.360791E+03	4.0960E+02
Mid_Car_4	1.683803E+05	5.644044E+05	1.338661E+03	2.356838E+01	1.500189E+03	3.9592E+02
Mid_Car_5	2.198726E+05	5.697038E+05	2.861918E+03	3.964090E+01	1.383223E+03	4.0605E+02
Mid_Car_6	1.875276E+05	5.665338E+05	1.590776E+03	5.390517E+01	1.438114E+03	3.9165E+02
Mid_Car_7	1.500681E+05	5.440397E+05	-9.221102E+03	9.274642E+01	1.438045E+03	3.6414E+02
End car_8	2.561603E+04	4.938548E+05	3.194339E+04	3.546731E+02	8.383062E+02	1.6956E+02

5.1.5 Case_5: Flow distributions at yaw-angle (β = 60°)

In the same fashion of case-4 except increased force values, pressure loads are still dominant than friction loads at wind yaw-angle much more. In Figure 14, Figure 15 and Table. 7 explained qualitatively and quantitatively aerodynamic resistance loads strongly hit high-speed train which is vulnerable to overturning incidents. In addition to that the wake regions are stronger at each car than the other cases. In this case, the friction resistances toward x-axis and y-axis components became more significant compared to all previous cases. The underbody and embankment interaction can be a cause of strong negative pressure drag at leeward side of each car accordingly.

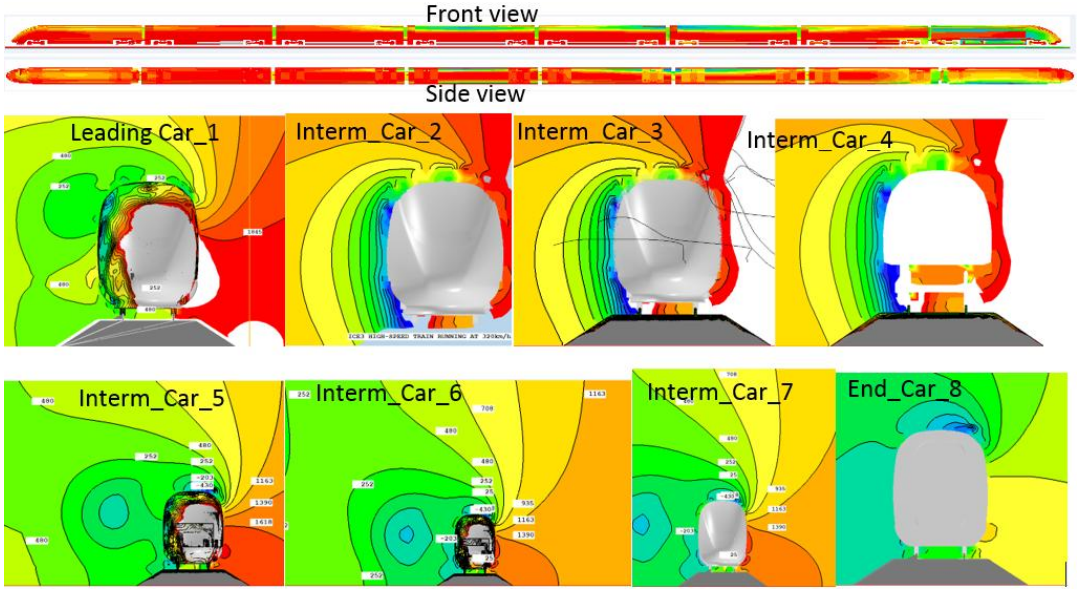

Figure 14: Aerodynamic resistance load distribution on ICE3 full-scaled and cross-sectional areas of train at yaw-angle β = 60°

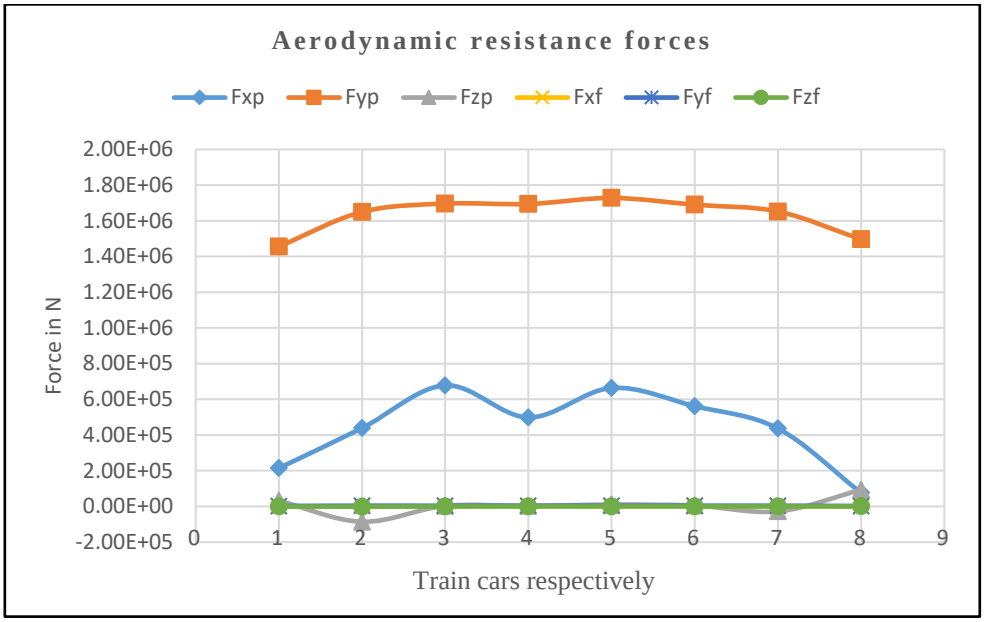

Figure 15: Comparison of the aerodynamic resistance forces value for each car at $\beta = 60°$

Table 7: Comparison of the aerodynamic resistance force values for each car at $\beta = 60°$

Car type	**Pressure Force (F_P) in N**			**Friction Force (F_f) in N**		
	Fxp	Fyp	Fzp	Fxf	Fyf	Fzf
Leading car_1	2.143400E+05	1.455613E+06	3.212482E+04	4.455375E+02	2.581396E+03	-2.58412E+02
Mid_Car_2	4.389485E+05	1.649945E+06	-8.555586E+04	9.916526E+02	4.081861E+03	-9.58649E+02
Mid_Car_3	6.781154E+05	1.696361E+06	3.010447E+03	1.132674E+03	3.723196E+03	-5.19650E+01
Mid_Car_4	4.984689E+05	1.694317E+06	2.709171E+03	1.086706E+03	4.177690E+03	6.089163E+01
Mid_Car_5	6.639159E+05	1.728113E+06	1.038695E+04	1.121513E+03	3.838068E+03	9.087513E+01
Mid_Car_6	5.618748E+05	1.690182E+06	4.964391E+03	1.084505E+03	4.003997E+03	2.020340E+02
Mid_Car_7	4.366699E+05	1.652037E+06	-2.771921E+04	1.018314E+03	4.063134E+03	2.717667E+02
End car_8	7.619734E+04	1.496566E+06	9.313785E+04	4.771356E+02	2.317455E+03	9.855989E+02

In Table 8 showed that the aerodynamic coefficient values of the ICE 3 full-scale train, the pressure drag one has decreased, and both lift and side coefficients increased due to increasing the wind yaw-angle attack on the train body. That's tested on the single track, standard embankment on the ground configuration. Those are the total train set values of aerodynamic coefficients of drag, side and lift forces. The study found out the maximum pressure drag in x-axis recorded when a wind yaw-zero and which is decreased as it increased. That's in the range of from 22.45% to minimum of

10.53% in each case. But, the side force is increased by from 66.36% to maximum of 97.38% and the lift force was recorded higher at yaw zero that was dropped in a very noticeable effects from case-1 to case-2 test by 98.48%. In the other hand, it started increase gradually while the wind yaw-angle increased, which were in the range of 21.64% to maximum of 69.15%. Besides, to determine running stability of ICE3 train lift and side force coefficients are very important.

Table 8: The aerodynamic total drag resistance on ICE3 train set

No. of test on Train set	Yaw-angle	Cd	C_S	C_L
1	$\beta = 0°$	1.38	0.21	77.87
2	$\beta = 15°$	1.18	8.00	1.18
3	$\beta = 30°$	0.98	35.95	3.15
4	$\beta = 45°$	0.76	106.86	4.02
5	$\beta = 60°$	0.68	320.29	13.03

6. Validation of the study

For validation purposes, we used EN14067-6:2010 standard report and experimental test values has compiled in Table 9. In HST aerodynamic analysis study the resistance coefficients have been compared those are the results taken from H. Kwon (2018) and R. Bagherwal (2018). Hence, the total drag coefficient in the CFD analyses having dropped down in the range of previous study results. Therefore, this study has analyzed and validated as shown in Table 9.

Table 9: Comparison of Aerodynamic resistance coefficients of HST by train dimensions used for validation

Case		Speed in km/h	Train dimensions		C_D
			Length	Area	
ICE3 at yaw angle 10° (Bagherwal, 2018)		320	1.529m	0.019 m^2	0.23
KTX-Sanchoen	By coasting test and empirical prediction methods (Kwon, 2018)	300	201m	9.335 m^2	0.957~1.341
HSR-350X		350	145m	9.335 m^2	0.715~0.965
KTX		300	388m	8.3044 m^2	2.061~2.529
HEMU-430X		430	149m	10.221 m^2	0.9~1.037
ICE3 end car	In a single track with ballast and rail wind tunnel coefficients at yaw angle 60° (En, 2009)	320		10 m^2	1.041
TGV Duplex power car				10 m^2	1.119
ETR 500 power car				10 m^2	0.857

7. Conclusion

The importance of aerodynamic performances is improving of efficiency of energy and driving stability. This study has presented and proposed two main important aerodynamic concepts for HST. First, when it comes to energy reduction, it found out pressure drag resistance is dominant than skin friction resistance in all test cases. The result depicted that a considerable amount of energy is not being dissipated as a form of heat through the interaction of air and train body surface. Thus, as the steady speed of 320km/h and exposed to wind at different yaw-angle, the skin friction component in aerodynamic resistance is negligible compared to pressure drag when the HST running in incompressible medium. Second, this paper also presented about HST stability effects under different wind yaw, which can have determined by cumulative lift and side forces in the tests.

As shown the study's results from case_1 to case_5 when the yaw-angle increase that weakens the skin friction resistance. Especially, when yaw-angle has been different from zero and increased value, the friction resistance has gone to negligible. It is possible to observe that the pressure drag coefficients high at zero-yaw and low at wind angle attacks of certain values. This is significantly sensitive to the position of the train on the embankment at the height of 1 m than the flat level track.

In summarized, as Table 8 showed that the aerodynamic coefficient values of the ICE 3 full-scale train, the pressure drag one has decreased, and both lift and side coefficients increased due to increasing the wind yaw-angle attack on the train body. That's tested on the single track, standard embankment on the ground configuration. Those are the total train set values of aerodynamic coefficients of drag, side and lift forces. The study found out the maximum pressure drag in x-axis recorded when a wind yaw-zero and which is decreased as it increased. That's in the range of from 22.45% to minimum of 10.53% in each case. But, the side force is increased by from 66.36% to maximum of 97.38% and the lift force was recorded higher at yaw zero that was dropped in a very noticeable effects from case-1 to case-2 test by 98.48%. In the other hand, it started increase gradually while the wind yaw-angle increased, which were in the range of 21.64% to maximum of 69.15%. Besides, to determine running stability of ICE3 train lift and side force coefficients are very important.

The results provided and captured insight into the flow around ICE3 HST that the pressure drag is importantly increased within yaw-angle increased. But, it would have showed that the friction loads on train car bodies have reversed. The train and its car stabilities didn't include the detailed in this study except has explained two main causes of train instability, which example of HST overturning forces are higher when wind attach angle is in more, those are aerodynamic lift and side forces and their coefficients.

Therefore, as the study concluded that some components of pressure drag resistance ultimately dominant over train body surface friction resistance when the HST running under incompressible fluid medium. It analyzed that the friction resistance load dramatically decreased while the train exposed to side winds.

Availability of Data and Materials

Author Contributions

Kibret Yilak Molla were in charge of the whole trial; Kibret wrote the manuscript, improved and checked all analysis.

Author information

Dr. Kibret Yilak Molla, born in 1987, is an assistant professor in the Department of Mechanical Engineering at University of Gondar, Ethiopia. He is working at Institute of Technology, mechanical engineering. He received his BSc. of mechanical engineering from Arba Minch University and MSc. of mechanical and Automotive engineering from Adama science and Technology, Ethiopia. PhD. In Seoul National Uinveristy of Science and Technology, South Korea. His research interests are Railway Vehicle System Dynamics, Aerodynamics, and Vehicle Structural Design and Automotive Engineering.

Declaration of Conflicting Interests

The author declare that they have no conflicts of interest.

Funding

The author received no financial support for the research, authorship, and/or publication of this article.

10. Appendix 1. Notations

Notation	Description
ICE	InterCity Express
HST	High Speed Train
TIS	Technical Standard for Interoperability
EN	Euro Norm
RSSB	Rail Safety and Standards Board
CFD	Computational Fluid Dynamics
VR	Virtual Reality
PHOENICS	Parabolic Hyperbolic Or Elliptic Numerical Integration Code Series
LES	Large Eddy Simulation
DES	Detached Eddy Simulation
RANS	Reynolds-Average Naiver-Stroke
F_x	Drag Force
F_y	Side Force
F_z	Lift Force
F_P	Pressure force
F_f	Friction force
dx	Center of pressure distance in the x-direction form center of gravity
dy	Center of pressure distance in the y-direction form center of gravity
dz	Center of pressure distance in the z-direction form center of gravity
C_x	Drag Coefficient
C_y	Side Coefficient
C_z	Lift Coefficient
A	Reference Area
L	Reference Normalization Length

V	Train Speed
$\vec{U}$	Wind Speed
$\vec{R}$	Wind to train relative speed
β	Wind to train speed relative angle
M_x	Rolling moment
M_y	Pitching moment
M_z	Yawing moment
C_{mx}	Rolling moment coefficient
C_{my}	Pitching moment coefficient
C_{mz}	Yawing moment coefficient
Eq.	Equation
Fig.	Figure
Fxp	Pressure force in x-axis
Fyp	Pressure force in y-axis
Fzp	Pressure force in z-axis
Fxf	Friction force in x-axis
Fyf	Friction force in y-axis
Fyf	Friction force in z-axis

Acknowledgements

The authors gratefully acknowledge the support of the Korean National University of Transportation and Seoul National University of Science and Technology. Thank you very much professor Hyeokbin Kwon, in Korea National University of Transportation and professor Jeong Seo Koo in the department of Railway Safety Engineering at Seoul National University of Science and Technology for your supporting me valuable ICE-3 train data and your incredible comments and editing this article.

8. References

Avila-Sanchez, S., Pindado, S., Lopez-Garcia, O., & Sanz-Andres, A. (2014). Wind tunnel analysis of the aerodynamic loads on rolling stock over railway embankments: The effect of shelter windbreaks. *Scientific World Journal*, *2014*. https://doi.org/10.1155/2014/421829

Bagherwal, R. (2018). *Numerical Simulation of Transient Aerodynamic Phenomena during Crosswind flow on High Speed Train.*

Baker, C., Cheli, F., Orellano, A., Paradot, N., Proppe, C., & Rocchi, D. (2009). Cross-wind effects on

road and rail vehicles. *Vehicle System Dynamics*, *47*(8), 983–1022. https://doi.org/10.1080/00423110903078794

Baker, C. J. (2014a). A review of train aerodynamics Part 2 - Applications. *Aeronautical Journal*. https://doi.org/10.1017/S0001924000009179

Baker, C. J. (2014b). A review of train aerodynamics Part 2 - Applications. *Aeronautical Journal*, *118*(4070). https://doi.org/10.1017/S0001924000009179

Cheli, F., Corradi, R., Rocchi, D., Tomasini, G., & Maestrini, E. (2010). Wind tunnel tests on train scale models to investigate the effect of infrastructure scenario. *Journal of Wind Engineering and Industrial Aerodynamics*, *98*(6–7), 353–362. https://doi.org/10.1016/j.jweia.2010.01.001

Cheli, F., Rocchi, D., Schito, P., Tomasini, G., & Masa, L. (n.d.). *Steady and moving high-speed train crosswind simulations . Comparison with wind-tunnel tests* . 1–12.

Coming, P. (2006). *The Railways (Interoperability) Regulations 2006*. *397*.

Commission, T. H. E. E. (2019). *COMMISSION IMPLEMENTING REGULATION (EU) 2019/773 of 16 May 2019*. *2004*(881).

Diedrichs, B. (2003). On computational fluid dynamics modelling of crosswind effects for high-speed rolling stock. *Proceedings of the Institution of Mechanical Engineers, Part F: Journal of Rail and Rapid Transit*, *217*(3), 203–226. https://doi.org/10.1243/095440903769012902

Diedrichs, B., Sima, M., Orellano, A., & Tengstrand, H. (2007). Crosswind stability of a high-speed train on a high embankment. *Proceedings of the Institution of Mechanical Engineers, Part F: Journal of Rail and Rapid Transit*, *221*(2), 205–225. https://doi.org/10.1243/0954409JRRT126

E P U B L I C O F U L G a R I a. (2009).

En, B. S. (2005). Railway applications — Testing for the acceptance of running characteristics of railway vehicles — Testing of running behaviour and stationary tests. *Communities*, *3*.

En, B. S. (2009). *Railway applications — Gauges*.

European Commission. (2003). *The Trans-European High-Speed Rail System: Guide for the application of the High-Speed TSIs*.

Huo-yue, X., Yong-le, L., Bin, W., & Hai-li, L. (n.d.). *Effect of wind barrier on the steady aerodynamic characteristic of trains by numerical simulation*. *Chu 2013*.

Kumar, K., Panchal, H., & Chauhan, R. (2016). A review on aerodynamic study of vehicle body using CFD. *Ncevt 2014*, *April 2014*.

Kwon, H. (2018). A study on the resistance force and the aerodynamic drag of Korean high-speed trains. *Vehicle System Dynamics*, *56*(8), 1250–1268. https://doi.org/10.1080/00423114.2017.1410184

Mohammad Mehdi Rashidi; Alireza Hajipour; Tian Li; Z. Yang; Qiliang Li. (2019). A Review of

Recent Studies on Simulations for Flow around High-Speed Trains. *Journal of Applied and Computational Mechanics*, *5*(2), 311–333. https://doi.org/10.22055/JACM.2018.25495.1272

Mueller, T. J., & DeLaurier, J. D. (2003). a Erodynamics of S Mall V Ehicles . *Annual Review of Fluid Mechanics*, *35*(1), 89–111. https://doi.org/10.1146/annurev.fluid.35.101101.161102

Noguchi, Y., Suzuki, M., Baker, C., & Nakade, K. (2019). Numerical and experimental study on the aerodynamic force coefficients of railway vehicles on an embankment in crosswind. *Journal of Wind Engineering and Industrial Aerodynamics*, *184*(April 2018), 90–105. https://doi.org/10.1016/j.jweia.2018.11.019

Raghunathan, R. S., Kim, H. D., & Setoguchi, T. (2002). Aerodynamics of high-speed railway train. In *Progress in Aerospace Sciences* (Vol. 38, Issues 6–7). https://doi.org/10.1016/S0376-0421(02)00029-5

RSSB. (2009). Resistance of Railway Vehicles to Roll-Over in Gales. *Group*, *June*, 1–28.

Sanquer, S., Barré, C., de Virel, M. D., & Cléon, L. M. (2004). Effect of cross winds on high-speed trains: Development of a new experimental methodology. *Journal of Wind Engineering and Industrial Aerodynamics*, *92*(7–8), 535–545. https://doi.org/10.1016/j.jweia.2004.03.004

Schober, M., Weise, M., Orellano, A., Deeg, P., & Wetzel, W. (2010). Wind tunnel investigation of an ICE 3 endcar on three standard ground scenarios. *Journal of Wind Engineering and Industrial Aerodynamics*, *98*(6–7), 345–352. https://doi.org/10.1016/j.jweia.2009.12.004

Sun, Z., Dai, H., Gao, H., Li, T., & Song, C. (2019). Dynamic performance of high-speed train passing windbreak breach under unsteady crosswind. *Vehicle System Dynamics*, *57*(3), 408–424. https://doi.org/10.1080/00423114.2018.1469777

Tian, H. (2019). Review of research on high-speed railway aerodynamics in China. *Transportation Safety and Environment*, *1*(1), 1–21. https://doi.org/10.1093/tse/tdz014

Yu, M., Jiang, R., Zhang, Q., & Zhang, J. (2019). Crosswind Stability Evaluation of High-Speed Train Using Different Wind Models. *Chinese Journal of Mechanical Engineering*, *32*(1). https://doi.org/10.1186/s10033-019-0353-7